Formation of free-standing magnetic particles by solid-state dewetting of $Fe_{80}Pd_{20}$ thin films

Gabriele Barrera[a,*], Federica Celegato[a], Marco Coïsson[a], Matteo Cialone[a,b], Paola Rizzi[b], Paola Tiberto[a]

[a]*Nanoscience and materials Divisions, INRiM, Torino,Italy*

[b]*Chemistry Department and NIS, University of Torino, Torino, Italy*

*Corresponding author (G. Barrera)..
E-mail address: g.barrera@inrim.it; Postal address: INRiM, Strada delle Cacce, 91, 10135, Torino, Italy.

Abstract

An alternative process to produce magnetic FePd nanoparticles dispersed in liquid solution exploiting a "top-down" strategy is here reported. This process is based on the solid-state dewetting of a $Fe_{80}Pd_{20}$ thin film to produce magnetic isolated islands array attached on a solid substrate. The subsequent detachment from the substrate offers the possibility to obtain free-standing magnetic nanoparticles for different applications. An adequate choice of the initial thickness of $Fe_{80}Pd_{20}$ thin film, annealing time and annealing temperature allows to finely tune the final size and shape of free-standing magnetic nanoparticles. A detailed study on the influence of latter parameters on islands morphology is here presented by SEM images analysis whereas the Johnson-Mehl-Avrami model is employed to extract the kinetics parameters of dewetting process. Room-temperature hysteresis loops and first-order reversal curves are measured in order to investigate the evolution of magnetic properties as a function of dewetting stage.

Keywords: Solid-state dewetting, magnetic nanoparticles, FePd alloy, magnetic thin film.

1. Introduction

The still growing interest in magnetic nanoparticles (MNPs) is mainly focused on the ability to produce them in a very controlled way [1-4]. In fact, a large variety of sizes, shapes, chemical compositions, and structures of MNPs is daily available, and their application gains increasingly attraction in a wide range of disciplines such as catalysis [5], biomedicine [6], and environmental remediation [7]. In this context, a number of suitable methods have been developed for the synthesis of MNPs exploring both physical and chemical techniques [3, 8]. The conventional mostly used chemical methods are low-cost methods allowing to synthesize high volumes of nanoparticles, nevertheless, their major drawback regards the complexity to use some elements and especially combine them in alloys during chemical reactions in order to obtain the desired properties.

To overcome such limitations, some recent studies have demonstrated the viability to use “top-down” approaches, applicable to a wide range of materials and alloys, to fabricate specifically designed MNPs [8, 9]. Usually, these “top-down” approaches involve lithography and etching process, which offer defined morphologies and uniform size of the nanostructures but suffer from high complexity and not negligible processing costs.

In this work, an easy-to-use “top-down” process to produce free-standing magnetic nanoparticles based on the solid-state dewetting of a magnetic thin film is reported. The solid-state dewetting is a thermally activated process where a thin film agglomerates to form an array of islands on a solid substrate upon annealing at temperatures below the melting point [10-13]. The dewetting effect is usually considered as a drawback that limits the fabrication of microelectronic devices based on thin films [14] but also as an alternative route, applicable to a wide range of materials and alloys, to nanostructure thin films obtaining well-controlled island arrays commonly used in areas such as catalysis, electronics, and plasmonics [15, 16]. Moreover, the detachment of islands from the substrate and their dispersion in a liquid solution represents an alternative and unconventional route to obtain free-standing MNPs.

The morphological evolution during the dewetting process from a highly anisotropic 2D shape of continuous thin film to a more isotropic 3D sphere-like shape of the isolated islands is driven by the minimization of the free-energy related to the interfaces between the film and its substrate. The starting point is the formation of holes into the film after an incubation time, it continues with the spontaneous growth of holes and it ends with holes junction and the formation of isolated islands [10, 11].

Many parameters appear to highly influence the size and density of the obtained islands as well as the kinetics of the dewetting, this prevents, from an experimental point of view, to single out the effect of one parameter from the others. Examples of these are: the initial thickness of thin film, the annealing temperature, the annealing time, the film crystallography, the number of defects in the film, etc. [10, 17].

As expected, the morphological transformation induced by the dewetting process determines also a consequent evolution of the magnetic properties. The magnetization does not lie anymore in a continuous film being constrained into isolated islands. The consequent increase of the surface/volume ratio leads to an increase of surface spin-disorder [18] and to an enhancement of magnetic surface anisotropy [19] resulting in a different reversal process of magnetization with respect to the one occurring in the continuous thin films. The magnetic behavior of islands is then maintained in the free-standing nanoparticles with some possible minor effect due to the stress release after detachment and/or to magnetic interaction among MNPs in the liquid solution.

In this work, polycrystalline $Fe_{80}Pd_{20}$ thin films were sputtered and then submitted to the solid-state dewetting process in order to form isolated FePd islands attached on substrate. The shape and size of islands was finely-tuned by means of the initial thickness of FePd thin film, annealing time and temperature resulting as a valid tool to meet the demands of various applications involving MNPs [6, 7]. In this context, free-standing FePd nanoparticles were produced and dispersed in liquid solution detaching the islands from the substrate. Room-temperature hysteresis loops and first-order reversal curves (FORCs) were measured on all samples in order to deeply understand the evolution of magnetic properties and the magnetization switching as a function of dewetting stage.

2. Experimental

$Fe_{80}Pd_{20}$ continuous thin films with nominal thickness of 30 and 100 nm were deposited by RF sputtering technique on Si[100] substrates covered with 500 nm of SiO_2. The as-prepared thin films were submitted to furnace annealing (heating rate ≈ 51 °C/min) in vacuum atmosphere (2 x 10^{-6} mbar) at selected temperatures T_A = 750, 820, 870 °C and for selected times ranging in the interval t_A = 0 – 100 minutes in order to promote the dewetting process.

Even if relatively high temperatures are reached during the heat treatments, a reaction between SiO_2 and FePd thin film is not expected due to the higher stability, as on oxide, of Si with respect to both Fe and Pd oxides in the Ellingham Diagram in which free energy of formation (ΔG) of metal oxides are reported versus temperature [20]. Furthermore, the high vacuum atmosphere reduces the presence of oxygen in the furnace chamber severely reducing the oxidation of the FePd surface during the annealing treatments.

The isolated magnetic islands formed from the sample with initial film thickness of 30 nm dewetted at 870 °C for 55 min were detached from the substrate by a high power ultrasonic sonication in acetone in order to obtain free-standing FePd nanoparticles.

Samples morphology of still attached or detached islands from the substrate was studied by scanning electron microscopy (SEM) equipped with a scanning transmission electron microscopy (STEM) detector. SEM images were analysed by an open source software *imagej* [21] in order to evaluate the area and the circularity of the magnetic islands.

Room-temperature hysteresis loops were measured by an alternating gradient field magnetometer (AGFM) operating in the field range -18 kOe < H < 18 kOe in the parallel and perpendicular configuration. A detailed description of the reversible and irreversible mechanisms of the magnetization switching was performed measuring the first-order reversal

curves by AGFM with the magnetic field applied in the film plane direction. The corresponding color plots were extrapolated from FORC experimental curves by an ad-hoc developed analysis procedure.

Room-temperature hysteresis loop of the free-standing FePd nanoparticles in acetone solution was measured by using a vibrating sample magnetometer (VSM) operating in the field range -17 kOe < H < 17 kOe equipped by a sample-holder able to accommodate liquid samples.

3. Results and Discussion

3.1 Morphological analysis

The morphological evolution of $Fe_{80}Pd_{20}$ thin film as a function of annealing time (t_A) during isothermal treatment at T_A = 870 °C is shown in Fig. 1. After 20 minutes of annealing (Fig. 1a), the film morphology evolves towards nucleation of holes having irregular shape heterogeneously distributed in the film inducing the exposure of the underlying SiO_2/Si substrate. The holes formation is most likely located at the grain boundaries of the as-deposited polycrystalline thin film with higher energy [22, 23]. Increasing the annealing time, the holes spontaneously grow by expelling film-matter; as a consequence, the exposed area of underlying substrate continuously increases. The growth of the holes during the dewetting process should be favoured by the vacuum atmosphere in which the samples are annealed [24].

In this context, different approaches have been presented in literature to describe the hole formation and propagation. Some of them are based on surface diffusion mechanisms leading to rapid growth of rims along the holes [25, 26]; others suggest the expansion of holes with a consequent growth of selected grains normal to the substrate [27]. More in general, several models based on capillary and growth approach are usually developed [24]. However, a deeper analysis of the holes propagation mechanism lies outside this work.

The holes propagation ends with their interconnection and the creation of isolated islands as shown in Fig. 1b, where, at t_A = 30 minutes, the holes are just interconnected and the formation of isolated FePd islands with irregular shape is observed. The increase of t_A up to 100 minutes leads to increase the islands size by means of coarsening process [28] and to develop a more spherical shape (Fig. 1c) through a process in which the free-energy is reduced and the system approaches to equilibrium [29].

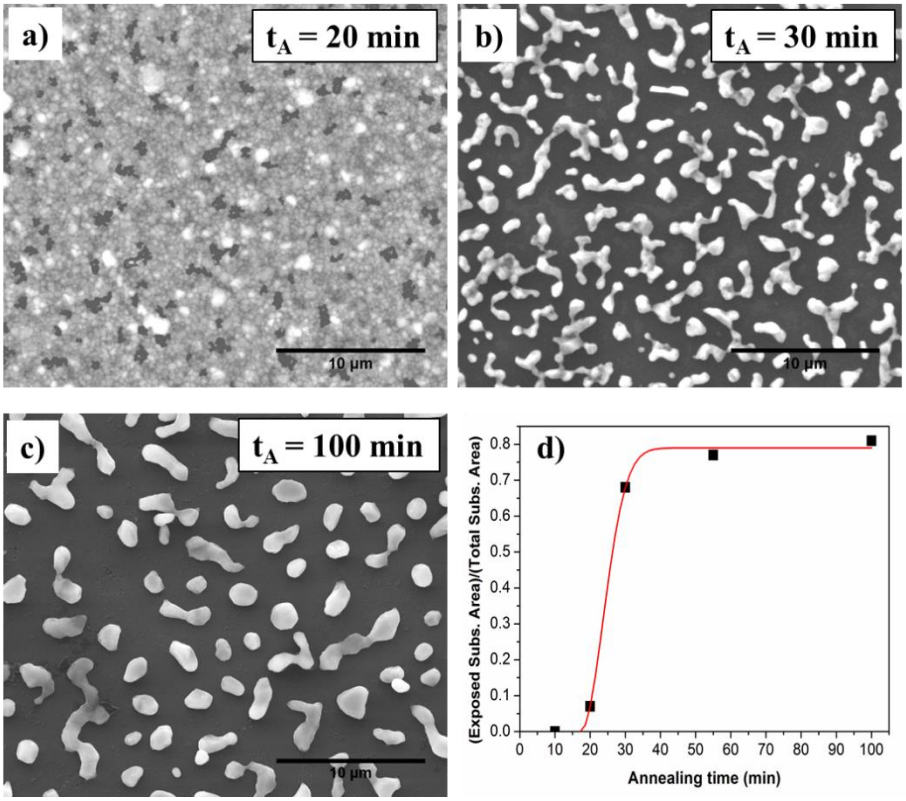

Figure 1. a) – c) FePd thin film (t = 100 nm) morphology after annealing at T_A = 870 °C for selected t_A: 20, 30 and 100 minutes; d) fraction of exposed substrate area as a function of t_A (black square) according to Johnson-Mehl-Avrami model (red line).

The time-evolution of exposed SiO_2/Si substrate area as a function of annealing time can be described by the Johnson-Mehl-Avrami model [30]:

$$Area_{exp}(t) = A\left(1 - e^{-N_h \pi v_h^2 (t-t_i)^2}\right)$$

where $Area_{exp}(t)$ is the fraction of exposed substrate area, A the saturation value of the process, N_h is the holes number per unit area, v_h is the growth rate of holes and t_i is the hole incubation time. N_h is considered to be temperature-independent [30] and is experimentally determined from morphological analysis of several SEM images of sample annealed for t_A = 20 minutes (Fig. 1a) resulting in the value of 1.7 x 10^{11} holes/m^2 that it is comparable to values obtained for other metallic materials [31].

By fitting the experimental data to Eq. 1 (see Fig. 1d), the kinetic parameters of the dewetting process i.e. the saturation value A, the growth rate of holes v_h and the holes incubation time t_i have been estimated: A = 0.79, v_h = 2.5 nm/s and t_i = 17.3 minutes. Therefore, the FePd thin film remains continuous without holes presence if the annealing time is shorter than t_i, as confirmed by SEM image of the sample annealed for just t_A = 10 minutes (Fig. S1 in the supplementary material). A more comprehensive study, to be done in future works, of the dewetting process on this alloy would require

performing the Johnson-Mehl-Avrami analysis on systems characterized by several sample thickness and different annealing temperature; in particular, this would allow to obtain the evolution of the dewetting velocity and the activation energy [32].

Several SEM images of samples morphology annealed at selected times (a collection is shown in Fig. 1 and in Fig. S1) have been analyzed in order to calculate the area distribution of isolated magnetic islands formed by the dewetting process. The islands formed after $t_A \approx 30$ minutes are characterized by an area distribution (Fig. 2a, red histogram) fitted by Lorentz curve (Fig. 2a, red solid line) with a peak at about 0.47 μm^2 and its half-width at half-maximum (HWHM) of about 2.13 μm^2; however, the islands shape is very irregular without a well-defined circularity distribution (Fig. 2b, red histogram). By increasing t_A, the area distribution becomes sharper with a slight decrease of HWHM (1.96 and 1.87 μm^2 for 50 and 100 min, respectively) and the peak moves to higher values (0.99 and 1.35 μm^2 for 50 and 100 min, respectively) as shown in Fig 2a. The observed increase in islands area is attributed to the coarsening effect that, during the dewetting process, induces a decrease of number of islands per unit area and an increase of their size [33]. Also the circularity distribution changes by increasing t_A resulting in a well-defined peak close to 1 (Fig. 2b) that indicates how the islands have become more similar to circles. The high circularity of the sample annealed for 100 min (Fig. 2b, blue histogram) allows to transform the corresponding area distribution into a diameter distribution fitted by a Lorentz curve with the most probable island diameter around 1.38 μm (inset in Fig. 2b).

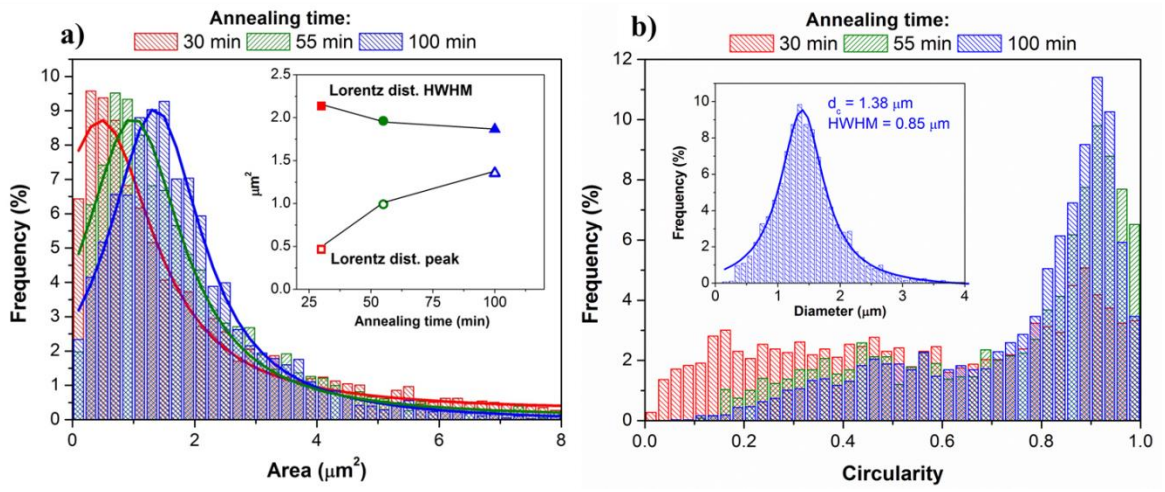

Figure 2. a) Islands area distribution formed at T_A = 870 °C and for different t_A fitted with the corresponding Lorentz curve (solid line); inset: evolution of peak and HWHM of Lorentz curve as a function of t_A. b) Islands circularity distribution formed at T_A = 870 °C and for different t_A; inset: islands diameter distribution formed at T_A = 870 °C for t_A = 100 minutes with the corresponding Lorentz curve (solid line).

A different way to control the thermal activated dewetting process is to change T_A. Its reduction from 870 °C to 750 °C keeping constant t_A = 55 minutes inhibits the dewetting process and the consequent islands formation in the FePd sample with thickness of 100 nm, as the thermal energy provided to the system is no longer sufficient to activate the dewetting process. The SEM images confirming the inhibition induced by the reduction of T_A are shown in Fig. S2 of the supplementary material where the FePd thin film annealed at 750 °C for 55 minutes is observed to remain continuous.

Conversely, the same thermal energy (T_A = 750 °C and t_A = 55 minutes) provided to FePd sample with a thickness of 30 nm annealed is now enough to induce the formation of isolated magnetic islands (Fig. 3a). The islands shape is very irregular indicating that the holes have just joined together and the agglomeration of the magnetic material into circular shape is starting. Increasing the annealing temperature (T_A = 820 and 870 °C) and keeping fixed t_A = 55 minutes (Fig. 3b and 3c), the rise of thermal energy lead to an increasingly circular islands shape.

The high circularity of magnetic islands of both samples annealed at higher temperature (the corresponding circularity distributions are shown in Fig. S3) allows to calculate their diameter distribution (Fig. 3d, green and blue bars for 820 and 870 °C, respectively) characterized by a Lorentz curve (Fig. 3d, solid lines) having a peak around 490 and 407 nm and a HWHM of about 354 and 315 nm for T_A = 820 and 870 °C sample, respectively.

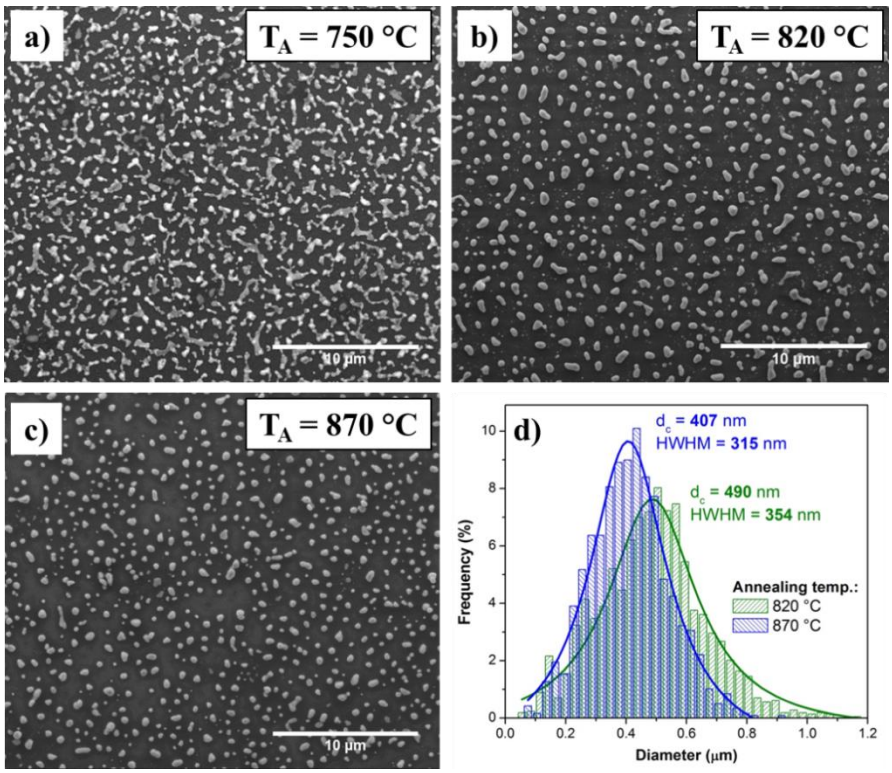

Figure 3. a) – c) FePd thin film (t = 30 nm) morphology after annealing for t_A = 55 minutes at selected temperature (T_A): 750, 820, and 870 °C; d) islands diameter distribution of sample b) and c).

These evidences, in addition to the comparison between the morphological of 30 nm (Fig. 3c) and 100 nm samples (Fig. S1) both annealed with the same condition (T_A = 870 °C and t_A = 55 min), reveal that the size, the density and interparticle distance of islands are strongly affected by the initial thickness of FePd thin film, as already observed in Au films [34] or Co films [35].

3.2 Magnetic characterization

Room-temperature in-plane hysteresis loops of as-deposited FePd samples with thickness of 100 nm is shown in Fig. 4a (black curve). The magnetization reversal process is typical of a soft magnetic material characterized by a single irreversible jump of magnetization with small coercive field (H_c ≈19 Oe), high magnetization remanence (M_r/M_{5kOe} ≈ 0.8) and a high susceptibility at coercive field ($\chi_c \approx 3.1 \times 10^{-5}$ Oe^{-1}).

After dewetting the FePd samples at T_A = 870 °C for selected annealing times, this magnetization jump becomes less marked and the magnetization reversal takes place on an increasingly wider magnetic field range with increasing t_A (Fig. 4a) resulting in a strong reduction of M_r/M_{5kOe} and of coercive susceptibility χ_c (inset of Fig. 4a). In particular, the hysteresis loop in the FePd sample annealed for 100 nm, so after the formation of isolated islands, shows an almost complete disappearance of the magnetization irreversible jump with low values of $M_r/M_{5kOe} \approx 0.03$ and $\chi_c \approx 1.3 \times 10^{-6}$ Oe^{-1} indicating that the magnetization reversal occurs mainly through reversible mechanisms.

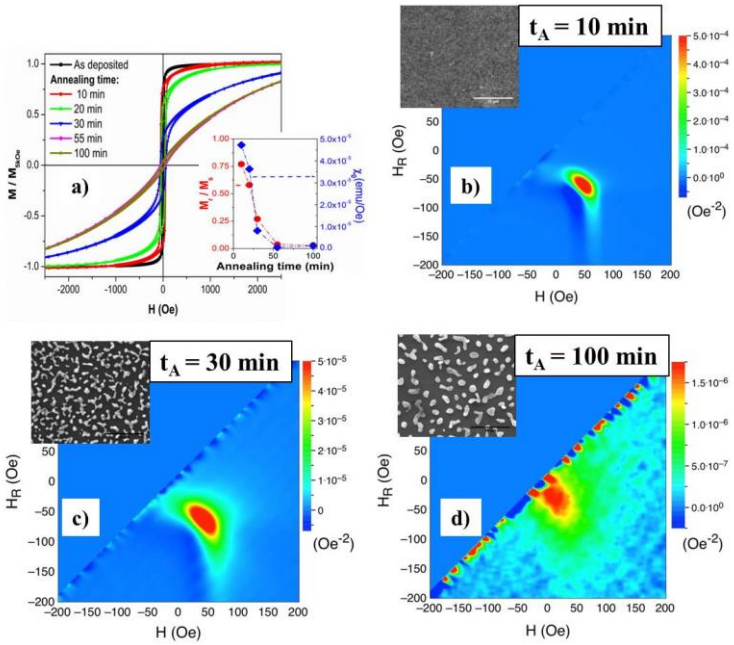

Figure 4. a) Normalized room-temperature hysteresis loops of as-deposited and dewetted samples at T_A = 870 °C for selected t_A, inset: magnetization remanence and coercive susceptibility as a function of t_A; b) - d) FORCs colour plot of dewetted samples at T_A = 870 °C for selected t_A, inset: SEM image of the corresponding sample.

To give an overall figure of magnetic behaviour, the reversible and irreversible mechanisms of the magnetization switching have been analysed by measuring FORCs on dewetted samples [36]. FORCs distributions are plotted by using a colour plot (ρ is the intensity of the colour map). The selected colour plots of samples annealed at t_A =10, 30 and 100 minutes are shown in Fig. 4 (b-d), respectively. In the colour plot of sample annealed for 10 minutes (Fig. 4b), so before the holes start to form, ρ displays a prominent peak in proximity of coercive field indicating a sharp and intense irreversible switching of magnetization. In addition, ρ assumes negative values (a dark blue halo located at H ≈ 35 Oe and $H_R \approx$ - 80 Oe near the peak) resulting from a magnetic interaction among different domains in the continuous thin film [37]. By increasing t_A up to 100 minutes, the ρ peak becomes progressively less intense and broader (Fig. 4c and 4d) demonstrating that the irreversible mechanisms of magnetization reversal are weaker and take place on a wider magnetic field range. This evidence is in good agreement with the observed reduction of M_r/M_{5kOe} and of χ_c observed in the hysteresis curve of the same sample (inset of Fig. 4a). Moreover in the colour plot of sample annealed at t_A = 100 minutes (Fig. 4d), the negative halo has completely disappeared indicating an absence of magnetic interactions both intra- that inter- isolated islands.

Room-temperature hysteresis loops of FePd samples with initial thickness of 30 nm in as-deposited continuous state and after dewetting at T_A = 870 °C for t_A = 55 minutes are measured both in-plane and out-of-plane configuration (Fig. 5a). The in-plane hysteresis curve of as-deposited thin film (blue curve) is characterized by a rather square shape with an intense magnetization jump located at the coercive field (≈ 20 Oe) and by a small value of applied magnetic field required to reach the saturation (M_s). This behaviour is typical of soft magnetic films in which the magnetization reversal is mainly governed by domain wall motion and the shape anisotropy induces the magnetization easy-axis to lie in the film plane [38]. Conversely, the out-of-plane hysteresis curve (orange curve) displays an almost linear behaviour of magnetization as a function of applied magnetic field not reaching the M_s even at the maximum applied value of 15 kOe indicating that this direction is a hard-axis of magnetization and the magnetization reversal occurs completely by magnetization rotation in the direction of the applied magnetic field [38].

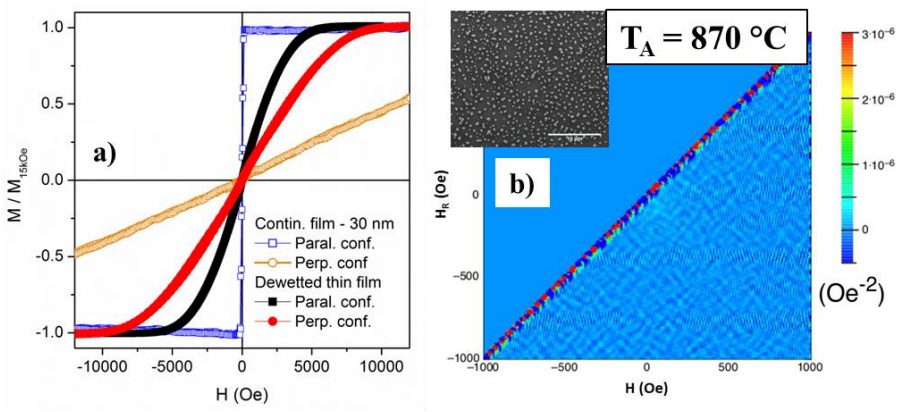

Figure 5. a) normalized room-temperature hysteresis loops of FePd samples (t = 30 nm) in as-deposited continuous state (blue and orange curve) and after dewetting at T_A = 870 °C for t_A = 55 minutes (red and black curve) measured both in-plane and out-of-plane configuration. b) FORC colour plot of sample dewetted at T_A = 870 °C for t_A = 55 minutes, inset: SEM image of the sample.

The remarkable difference in shape between the magnetization curves measured in the two directions indicates that a large amount of energy must be spent to move the magnetization away from its easy-axis and to saturate the sample in its hard-axis [35]. This energy, provided by the external applied magnetic field, is related to the sample magnetic effective anisotropy energy (E_{eff}) and can be evaluated by calculating the area enclosed between the first branch of the in-plane hysteresis loop and the first branch of out-of-plane one in the field interval from zero to the magnetic field required to completely saturate the magnetization in both directions [38]. The estimate E_{eff} value for as-deposited film results to be around 12.9 kOe.

The dewetting process (T_A = 870 °C and t_A = 55 min) changes the sample morphology starting from a highly anisotropic 2D shape of continuous thin film to the more isotropic 3D sphere-like shape of the islands. This morphology transformation induces a rearrangement of magnetization that is not forced into film plane any more but it lies now into islands giving rise to also a more isotropic magnetic behaviour. In fact, the shape of in-plane and out-of-plane hysteresis curves is similar (Fig. 5a) and both reach the saturation with an applied magnetic field below 10 kOe [35]. The in-plane direction could be still considered an easy-axis of magnetization respect to the out-of-plane one due to the higher χ_c and the lower value of applied magnetic field required to reach the saturation. Nevertheless, the E_{eff} estimated for these two direction is 1.67 kOe resulting in a huge decrease with respect to the highly anisotropic continuous thin film.

Moreover, the in-plane magnetization reversal in this dewetted sample is characterized by a complete absence of irreversible mechanisms as indicated by the very smooth hysteresis curve without sudden jumps (Fig. 5a, black curve). This evidence is also confirmed by the FORCs distribution without any visible peaks (Fig. 5b).

3.3 Free-standing FePd magnetic nanoparticles

The final step to obtain free-standing FePd magnetic nanoparticles is based on the detachment of magnetic islands from the SiO_2/Si substrate by a high power sonication in acetone.

In this work, free-standing FePd nanoparticles are obtained dewetting the FePd thin film with initial thickness of 30 nm at T_A = 870 °C for t_A = 55 min. These parameters have been chosen taking into account the results, presented in section 3.1 and 3.2, on solid-state dewetting kinetic process of thin films in order to obtain free-standing nanoparticles characterized by a circle shape, a nanometric size (see Fig. 3c and d) and a controlled magnetic behaviour.

The morphology of selected free-standing FePd nanoparticles imaged by STEM is shown in Fig. 6a and b. As expected, the detachment process does not damage the island morphology forming NPs with a well-defined contour. The difference in NPs diameter visible in Fig. 6a confirms the high HWHM value of diameter distribution (see Fig. 3d) calculated from the starting islands still attached on substrate.

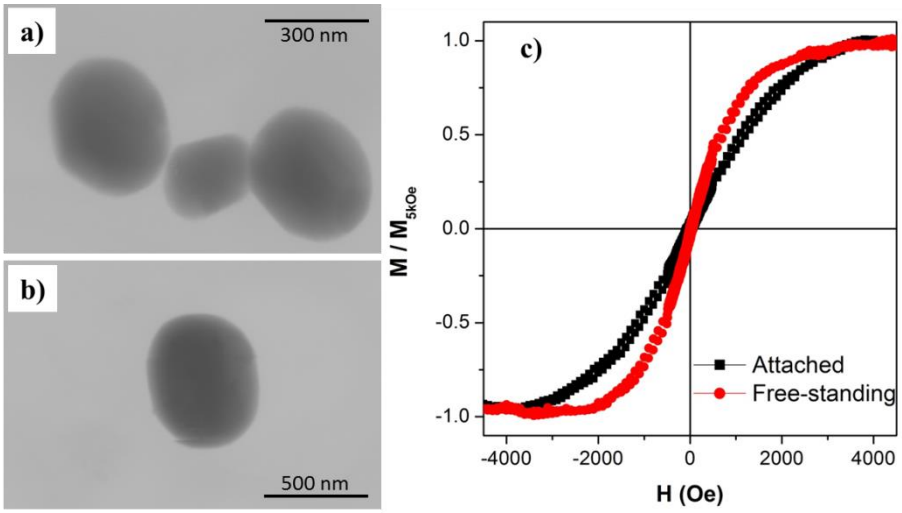

Figure 6. a) - b) STEM images of free-standing FePd nanoparticles; c) normalized room-temperature hysteresis loops of FePd islands still attached on the substrate (black curve) and subsequently dispersed in acetone (red curve).

The normalized room-temperature magnetization curve measured on FePd islands still attached on the substrate (black curve) and subsequently dispersed in acetone (red curve) are shown Fig. 6c. As already observed previously, the magnetization reversal of attached islands occurs with a gradual reduction of magnetization over a wide field interval resulting in low values of $\chi_c \approx 5.3 \times 10^{-4}$ Oe^{-1} and of $M_r/M_{5kOe} \approx 0.03$; whereas the coercive filed value is about $H_c \approx 73$ Oe. After the islands detachment and their dispersion in acetone, the corresponding magnetization reversal takes place on a smaller magnetic field interval increasing slightly the $\chi_c \approx 10.6 \times 10^{-4}$ Oe^{-1} and $M_r/M_{5kOe} \approx 0.04$ whereas the H_c is reduced to ≈ 37 Oe. The observed evolution of magnetic character after detachment and dispersion can be mainly

attributed to the NPs mobility inside the liquid medium and to the consequent random alignment of NPs with respect to the applied magnetic field during the measurement [8].

The absence of irreversible mechanisms in the magnetization process of free-standing nanoparticles with a smooth approach to saturation ensures a good two-way correspondence between the applied field and the magnetization value. This feature is of interest in different applications in which an accurate remote control of nanoparticles motion and displacement is crucial. In this context, drug delivery assisted by magnetic nanoparticles in biomedicine area is one of the most important applications based on this approach [39, 40]; finely controllable magnetization values would allow accurate direction of magnetic vectors (nanoparticles) loaded by drugs through the blood vessels towards a given target in the patient body. Furthermore, the increase of χ_c would also allow to reduce the strength of the external field exploited to drive the nanoparticles, therefore helping in addressing one of the main limitations of magnetic drug delivery technique [39].

Magnetic interaction among NPs in the liquid solution and/or stress release after detachment could contributed to the observed change in magnetic properties [33, 34]. However, this investigation lies outside of this preliminary work focused on the fabrication of MNPs by solid-state dewetting of thin film.

4. Conclusion

A process based on solid-state dewetting of thin film has been proposed to obtain free-standing FePd magnetic nanoparticles.

$Fe_{80}Pd_{20}$ thin films were sputtered on SiO_2/Si substrate and their initial thickness in combination with the annealing temperature and time have been used to control the resulting shape and size of isolated magnetic islands. Increasing the annealing time, the islands area distribution becomes sharper and the corresponding peak moves to higher values, and an enhancement of the islands circularity has been observed.

The morphological evolution during the dewetting process from a highly anisotropic 2D shape of continuous thin film to the more isotropic 3D sphere-like shape of the isolated islands induces a rearrangement of magnetization resulting in a weakening of irreversible mechanism of magnetisation curve.

Finally, morphological and magnetic properties are mostly maintained after the detachment of island from the substrate confirming the feasibility of this process as an alternative, easy and novel route to obtain free-standing magnetic nanoparticles.

Acknowledgements

Funding: This study has been carried out and financed in the framework of the European training network project SELECTA (ETN 642642).

References

[1] N.D. Burrows, A.M. Vartanian, N.S. Abadeer, E.M. Grzincic, L.M. Jacob, W. Lin, J. Li, J.M. Dennison, J.G. Hinman, C.J. Murphy, Anisotropic nanoparticles and anisotropic surface chemistry, J. Phys. Chem. Lett. 7 (2016) 632−641.

[3] P. Quaresma, I. Osório, G. Dória, P.A. Carvalho, A. Pereira, J. Langer, J. P. Araújo, I. Pastoriza-Santos, L.M. Liz-Marzán, R. Franco, P. V. Baptista, E. Pereira, Star-shaped magnetite@gold nanoparticles for protein magnetic separation and SERS detection, RSC Adv. 4 (2014) 3659–3667.

[3] T. Hyeon, Chemical synthesis of magnetic nanoparticles, Chem. Commun. (2003) 927–934.

[4] J-W. Moon, C.J. Rawn, A.J. Rondinone, L.J. Love, Y. Roh, S. M. Everett, R.J. Lauf, T.J. Phelps, Large-scale production of magnetic nanoparticles using bacterial fermentation, J. Ind. Microbiol. Biotechnol. 37 (2010) 1023–1031.

[5] M. B. Gawande, P.S. Branco R.S. Varma, Nano-magnetite (Fe_3O_4) as a support for recyclable catalysts in the development of sustainable methodologies, Chem. Soc. Rev. 42 (2013) 3371-3393.

[6] T.K.T. Nguyen, Magnetic nanoparticles from fabrication to clinical application, FL:CRC Press Taylor & Francis Group, Boca Raton, 2012.

[7] S.C.N. Tang, I.M.C. Lo, Magnetic nanoparticles: Essential factors for sustainable environmental applications, Water Res. 47 (2013) 2613-2632.

[8] P. Tiberto, G. Barrera, F. Celegato, G. Conta, M. Coïsson, F. Vinai, F. Albertini, $Ni_{80}Fe_{20}$ nanodisks by nanosphere lithography for biomedical applications, J. Appl. Phys. 117 (2015) 17B304.

[9] W. Hu, R.J. Wilson, A. Koh, A. Fu, A.Z. Faranesh, C.M. Earhart, S.J. Osterfeld, S.-J. Han, L. Xu, S. Guccione, R. Sinclair, S.X. Wang, High-moment antiferromagnetic nanoparticles with tunable magnetic properties, Adv. Mater. 20 (2008) 1479–1483.

[10] F. Leroy, Ł. Borowik, F. Cheynis, Y. Almadori, S. Curiotto, M. Trautmann, J.C. Barbé, P. Müller, How to control solid-state dewetting: A short review, Surf. Sci. Rep. 71 (2016) 391-409.

[11] C. V. Thompson, Solid-state dewetting of thin film, Annu. Rev. Mater. Res. 42 (2012) 399–434.

[12] M. Kang, S.-G. Park, K.-H. Jeong, Repeated solid-state dewetting of thin gold films for nanogap-rich plasmonic nanoislands, Sci. Rep. 5 (2015) 14790.

[13] O. Pierre-Louis, Solid-state wetting at the nanoscale, Prog. Cryst. Growth. Ch. 62 (2016) 177-202.

[14] S. Sharma, M.H. Rafailovich, D. Peiffer, J. Sokolov, Control of dewetting dynamics by adding nanoparticle fillers, Nano Lett. 1 (2001) 511-514.

[15] V.S. Makarov, V.A. Milichko, I.S. Mukhin, I.I. Shishkin, D.A. Zuev, A.M. Mozharov, A.E. Krasnok, P.A. Belov, Controllable femtosecond laser-induced dewetting for plasmonic applications, Laser Photonics Rev. 10 (2016) 91-99.

[16] L.-W. Wang, C.-F. Cheng, J.-W. Liao, C.-Y. Wang, D.-S. Wang, K.-F. Huang, T.-Y. Lin, R.-M. Ho, L.-J. Chena, C.-H. Lai, Thermal dewetting with a chemically heterogeneous nano-template for self-assembled $L1_0$ FePt nanoparticle arrays, Nanoscale 8 (2016) 3926-3935.

[17] P.D. Nsimama, A. Herza, D. Wanga, P. Schaaf, Influence of the substrate on the morphological evolution of gold thin films during solid-state dewetting, App. Surf. Sci. 388 (2016) 475–482

[18] F. Zeb, K. Nadeem, S.K.A. Shah, M. Kamran, I.H. Gul, L. Ali, Surface spins disorder in uncoated and SiO_2 coated maghemite nanoparticles, J. Magn. Magn. Mater. 429 (2017) 270–275.

[19] P.V.P. Madduri, S.N. Kaul, Core and surface/interface magnetic anisotropies in nanocrystalline nickel, J. Alloy Compd. 689 (2016) 533e541

[20] Young, D. J. High Temperature Oxidation and Corrosion of Metals, Elsevier, 2008.

[21] W. S. Rasband, IMAGEJ http://imagej.nih.gov/ij/.

[22] D.J. Srolovitz, S.A. Safran, Capillary instabilities in thin films. I. Energetics, J. Appl. Phys. 60 (1986) 247.

[23] N. Gazit, L. Klinger, E. Rabkin, Chemically-induced solid-state dewetting of thin Au films, Acta Mater. 129 (2017) 300-311.

[24] P. Jacquet, R. Podor, J. Ravaux, J. Lautru, J. Teisseire, I. Gozhyk, J. Jupille, R. Lazzari, On the solid-state dewetting of polycrystalline thin films: Capillary versus grain growth approach, Acta Mater. 143 (2018) 291-290.

[25] D. J. Srolovitz, S. A. Safran, Capillary instabilities in thin films. II. Kinetics, J. Appl. Phys. 60 (1986) 255-260.

[26] H. Wong, P. W. Voorhees, M. J. Miksis, S.H. Davis, Periodic mass shedding of a retracting solid film step, Acta Mater. 48 (2000) 1719-1728.

[27] O. Kovalenko, J.R. Greer, E. Rabkin, Solid-state dewetting of thin iron films on sapphire substrates controlled by grain boundary diffusion, Acta Mater. 61 (2013) 3148-3156.

[28] E.J. Luber, B.C. Olsen, C. Ophus, D. Mitlin, Solid-state dewetting mechanisms of ultrathin Ni films revealed by combining *in situ* time resolved differential reflectometry monitoring and atomic force microscopy, Phys. Rev. B, 82 (2010) 085407

[29] D.A. Porter, K.E. Easterling, Phase transformations in metals and alloys, Third Edition (Revised Reprint). (CRC Press, 1992)].

[30] E. Jiran, C. V. Thompson, Capillary instabilities in thin, continuous films, Thin Solid Films 208 (1992) 23.

[31] R. Esterina, X.M. Liu, A.O. Adeyeye, C.A. Ross, W.K. Choi, Solid-state dewetting of magnetic binary multilayer thin films, J. Appl. Phys. 118 (2015) 144902

[32] F. Cheynis, F. Leroy, T. Passanante, P. Müller, Agglomeration dynamics of germanium islands on a silicon oxide substrate: A grazing incidence small-angle x-ray scattering study, Appl. Phys. Lett. 102 (2013) 161603-1/4.

[33] F. Niekiel, P. Schweizer, S.M. Kraschewski, B. Butz, E. Spiecker, Acta Mater. The process of solid-state dewetting of Au thin films studied by in situ scanning transmission electron microscopy, 90 (2015) 118–132.

[34] Y. Kojima, T. Kato, Nanoparticle formation in Au thin films by electron-beam-induced dewetting, Nanotechnology 19 (2008) 255605.

[35] Y.-J. Oh, C.A. Ross, Y.S. Jung, Y. Wang, C.V. Thompson, Cobalt nanoparticle arrays made by templated solid-state dewetting, Small 5 (2009) 860–865.

[36] A. P. Roberts, C.R. Pike, K.L. Verosub, First-order reversal curve diagrams: A new tool for characterizing the magnetic properties of natural samples, J. Geophys. Res**.** 105 (2000) 28461-28475.

[37] I. Panagiotopoulos, A simple approach to the First-order Reversal Curves (FORC) of two-phase magnetic systems, J. Magn. Magn. Mater, 323 (2011) 2148-2153.

[38] B. D. Cullity, C.D. Graham, Introduction to magnetic materials, IEEE Press, John Wiley & Sons New Jersey, USA, 2009.

[39] M. Arruebo, R. Fernández-Pacheco, M. R. Ibarra, J. Santamaría, Magnetic nanoparticles for drug delivery, Nanotoday 2 (2007) 22-32.

[40] M. Angelakeris, Magnetic nanoparticles: A multifunctional vehicle for modern theranostics, BBA-Gen. Subjects 1861 (2017) 1642-1651.

[41] D Sander, The correlation between mechanical stress and magnetic anisotropy in ultrathin films Rep. Prog. Phys. 62 (1999) 809–858.

[42] P. Allia, G. Barrera, P. Tiberto, T. Nardi, Y. Leterrier, M. Sangermano, Fe_3O_4 nanoparticles and nanocomposites with potential application in biomedicine and in communication technologies: Nanoparticle aggregation, interaction, and effective magnetic anisotropy, J. Appl. Phys. 116 (2014) 113903.